the consequent Diels-Alder reaction of the cyclopentadiene with the more stable nadic group. At higher temperature, all these groups polymerize at basically the olefinic positions, forming a three-dimensional cross-linked polymer network (Scheme I).

Conclusion

The results of the solution and solid-state ^{13}C NMR study of the 2NE/MDA and PMR imides indicated that the polymerization mechanisms of these more complex imides are consistent with those found in the simpler, soluble imides, i.e., retro-Diels-Alder reaction of the end-capped nadic group and further Diels-Alder reaction of the oligomers and cyclopentadiene to form the various isomeric end-capped groups. These groups then polymerize through reaction of the nadic olefinic group to form the three-dimensional polymer network. This conclusion is derived from the mutually complementary data of solution and solid-state ^{13}C NMR and after comparison with the data of the polymerization of the simpler, single end-capped imide model compounds.

Solid-state ^{13}C NMR can be used to study the curing of polymers which are insoluble or only sparingly soluble in common NMR solvents. This can be especially effective if complementary solution NMR data are utilized in the study. High ^{1}H decoupling field, cross polarization, and MASS are essential in order to obtain reasonably high resolution ^{13}C NMR spectra of these amorphous solid polymers. It appears that little or no improvement in resolution of these amorphous polymers is observed with increasing static field in many cases; however, the expected increase in sensitivity is clearly observed.

Acknowledgment. We thank the National Aeronautics and Space Administration for supporting most of this work under Grants NSG3142 and NSG3241. We are grateful to Dr. Richard Lauver of NASA, Drs. William Moniz and Henry Resing of the Naval Research Laboratory and, Dr. Nan-I Liu of Case Western Reserve University for helpful discussions. Special thanks are due Dr. Liu for this effort in modifying the NT-150 spectrometer. We are also grateful to Mr. M. Zabel of Bruker-Physik, A. G. (West Germany), for taking the spectra on the CXP-300 spectrometer.

References and Notes

(1) Serafini, T. T.; Delvigs, P.; Lightsey, G. R. *J. Appl. Polym. Sci.* **1972**, *16*, 905.
(2) Burns, E. A; Jones, R. J.; Vaughn, R. W.; Kendrick, W. P. TRW-1126-6013-R.0-00, TRW Systems Group, Jan 1970. Also NASA CR-72633, 1970.
(3) Wong, A. C.; Ritchey, W. M. *Macromolecules*, preceding paper in this issue.
(4) Schaefer, J.; Stejskal, E. O. *J. Am. Chem. Soc.* **1976**, *98*, 1031.
(5) Lippmaa, E.; Alla, M.; Tuherm, T. *Magn. Reson. Relat. Phenom., Proc. Congr. Ampene, 19th, 1976* **1976**, 113.
(6) Garroway, A. N.; Moniz, W. B.; Resing, H. A. *Org. Coat. Plast. Chem.* **1976**, *36*, 133.
(7) Lowe, I. J. *Phys. Rev. Lett.* **1959**, *2*, 285.
(8) Andrew, E. R.; Badbury, A.; Eades, R. G. *Nature (London)* **1958**, *182*, 1659.
(9) Pines, A.; Gibby, M. G.; Waugh, J. S. *J. Chem. Phys.* **1973**, *59*, 569.
(10) Hartmann, S. R.; Hahn, E. L. *Phys. Rev.* **1962**, *128*, 2042.
(11) Andrew, E. R. *Prog. Nucl. Magn. Reson. Spectrosc.* **1971**, *8*, 1.
(12) Maricq, M.; Waugh, J. S. *Chem. Phys. Lett.* **1977**, *47*, 327.
(13) Stejskal, E. O.; Schaefer, J.; Steger, T. R. *Symp. Faraday Soc.* **1978**, *No. 12*.
(14) Mehring, M. *NMR: Basic Princ. Prog.* **1976**, *11*, Chapter IV.
(15) Earl, W. L.; VanderHart, D. L. *Macromolecules* **1979**, *12*, 762.

Dynamics of Dilute Polymer Solutions

L. K. Nicholson and J. S. Higgins*

Department of Chemical Engineering and Chemical Technology, Imperial College, London SW7 2BY, United Kingdom

J. B. Hayter

Institut Laue-Langevin, 38042 Grenoble Cedex, France. *Received November 12, 1980*

ABSTRACT: Polystyrene, poly(tetrahydrofuran), and poly(dimethylsiloxane) in dilute solution in C_6D_6 and in CS_2 have been observed by the neutron spin-echo technique. Motion over distances up to 30 Å has been measured with an energy resolution of 0.01 μeV ($\sim 10^7$ Hz). Systematic deviations from Q^3 behavior at higher frequencies have been fitted to theoretical predictions and characteristic length and frequency parameters extracted for each polymer.

1. Introduction

A linear polymer molecule in dilute solution adopts a random-coil configuration which is continuously changing as rotation about backbone bonds occurs. The driving force for this Brownian motion is the thermal energy and its rapidity depends both on the energy barriers to internal rotation of the bonds and on the viscous drag of the solvent.[1] The motion may be observed directly in scattering experiments where probe particles (neutrons or photons) exchange energy with the polymer molecules. Alternatively, the molecular motion of the polymer dominates the response of the solution to external applied forces, giving rise to the various moduli and the dynamic viscosity. The observation is strongly dependent on the frequency of the applied stress or the energy range covered by the scattering experiments. Brownian motion of the whole polymer molecule dominates scattering experiments at low energies, and only the overall molecular dimensions (e.g., the end-to-end distance $\langle r^2 \rangle$) and the solvent viscosity are important. At very high frequencies there is not time for cooperative bond rotations and the molecular response to stimulus is confined to local bending and stretching of the bonds. This motion is therefore highly dependent on the local chemistry of the polymer. Between these two extremes there lies a frequency range where measurement is sensitive to detailed changes in the coil conformation. Points on the chain not too far removed from each other have time to change their relative positions during the

0024-9297/81/2214-0836$01.25/0

observation. The continually changing molecular conformation causes fluctuations in the length of a chain segment (long enough to obey Gaussian statistics) and lead it to behave like a spring under tension. In models developed by Rouse[2] and Zimm,[3] the polymer molecule is represented by a series of such springs of length a connected by beads and the frictional effect of the solvent is confined to the beads. Rouse ignored hydrodynamic interactions between the beads through the solvent in the so-called free draining limit whereas the Zimm theory includes these hydrodynamic interactions. Pecora[4] and de Gennes[5] have calculated the scattering laws for Rouse and Zimm chains in the range $1/\langle r^2\rangle^{1/2} \ll Q \ll 1/a$, where Q is the change in wave vector defined in eq 2 below. The predictions for Zimm chains will be discussed in the next section.

For the Zimm model (and strictly for Θ conditions) the longest relaxation time τ_1 is defined by

$$\tau_1 = 0.2\eta_s\langle r^2\rangle^{3/2}/kT \tag{1}$$

where η_s is the solvent viscosity.

For polystyrene of molecular weight 50 000 in benzene (η_s = 0.56 cP at 30 °C), τ_1 from eq 1 is 1.3×10^{-7} s. Thus for dynamic modulus measurements Zimm internal motion will not be observed for ordinary solvents and modest molecular weights except at very high frequencies (which require special techniques). It has therefore become common to use high molecular weights and high-viscosity solvents,[6] thus increasing τ_1 to 10^{-1}–10^{-3} s. Results show a different behavior taking over at frequencies above $\sim 10/\tau_1$, where local motion apparently becomes important.

In scattering experiments the two techniques of particular importance for polymer solutions are photon correlation spectroscopy (PCS)[7] and neutron scattering.[8] The upper frequency limit of PCS is about 10^6 Hz. In order to observe Zimm modes in light scattering experiments, τ_1 has been increased via the molecular dimensions. For polystyrene with $M_w = 10^7$, $1/\tau_1$ is of the order 10^4 Hz. Good agreement with de Gennes' calculation for a chain undergoing internal Zimm motion has been observed.[9] Until recently, neutron scattering experiments have been confined to the frequency range above 10^9 Hz. In this range local bond rotation dominates, although some indication of Zimm-like motion has been observed.[10-12] The advent of the neutron spin-echo technique (NSE)[13-16] has extended the range of observation down to 10^7 Hz. NSE data have already been published showing Zimm motion for a very flexible polymer in dilute solution[17] and Rouse motion for a single chain in a polymer melt.[18] Using neutron scattering, one can now observe the transition from long-range internal motion to the local motion responsible for high-frequency limiting viscoelastic properties.

Akcasu et al.[19] have recently calculated the scattering from a polymer molecule in dilute solution over the whole frequency range (reproducing the de Gennes results at the intermediate frequencies). Excellent agreement between light scattering data and these predictions has been found for the range around $1/\tau_1$ covering the changeover from molecular difusion to internal modes. In this paper we present neutron data for the range $\gtrsim 10/\tau_1$, where local motion begins to take over from internal modes as the dominant process.

2. Neutron Scattering from Polymers in Dilute Solution

In a neutron scattering experiment the frequency ω is defined by the energy transfer from the scattered neutron

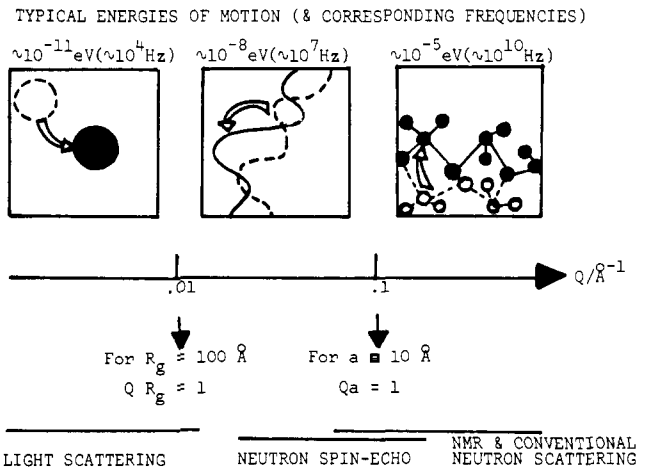

Figure 1. Pictorial representation of the molecular motion of a polymer chain. The numerical values correspond to a chain of radius R_g = 100 Å and step length a = 10 Å, for which $\tau_1 = 4 \times 10^{-7}$ s (assuming a solvent viscosity of 0.56 cP, i.e., benzene at 30 °C).

to the polymer molecules, $\Delta E = \hbar\omega$ ($\omega = 10^7$ Hz corresponds to ΔE = 0.007 μeV). In such a scattering experiment the observation depends not only on the energy transfer but also on the change in wave vector or momentum transfer, Q, which governs the spatial scale of observable motion. If λ is the neutron wavelength and $\mathbf{k}$ is the corresponding wave vector ($|\mathbf{k}| = 2\pi/\lambda$), then

$$\mathbf{Q} = \mathbf{k}_i - \mathbf{k}_f \tag{2}$$

where i and f refer to the incident and scattered beams, respectively. For elastic or quasi-elastic scattering (where $|\mathbf{k}_i| \approx |\mathbf{k}_f|$)

$$Q = |\mathbf{Q}| = (4\pi/\lambda)\sin\theta \tag{3}$$

where 2θ is the angle of scatter.

An indication of the distance scales corresponding to the various frequency ranges for polymer motion described in the previous section is given in Figure 1, together with the available scattering techniques. The Q value corresponding to the frequency $1/\tau_1$ where Zimm modes take over from molecular diffusion is $1/R_g$, where $R_g = (\langle r^2\rangle/6)^{1/2}$ is the radius of gyration of the polymer molecule, while the high-frequency behavior sets in around $Q = 1/a$, where a is the spring length in the Zimm model. Typical neutron wavelengths range from 1 to 10 Å and for dynamic measurements flux limitations preclude sufficient beam collimation for observation of scattering angles $2\theta \leq 2°$. Neutron observation therefore covers distances less than about 30 Å.

In a scattering experiment the cross section may contain contributions from both the coherent and incoherent scattering laws,[20] $S_{coh}(Q,\omega)$ and $S_{inc}(Q,\omega)$.[20,21] These are related to the space–time correlation function, $G(r,t)$, and the corresponding self-term, $G_s(r,t)$, by double Fourier transforms

$$S_{coh}(Q,\omega) = \int S_{coh}(Q,t)e^{i\omega t}\,dt = \int\int G(\mathbf{r},t)e^{i(\mathbf{Q}\cdot\mathbf{r}-\omega t)}\,d\mathbf{r}\,dt \tag{4}$$

$$S_{inc}(Q,\omega) = \int S_{inc}(Q,t)e^{i\omega t}\,dt = \int\int G_s(\mathbf{r},t)e^{i(\mathbf{Q}\cdot\mathbf{r}-\omega t)}\,d\mathbf{r}\,dt \tag{5}$$

$S_{coh}(Q,t)$ and $S_{inc}(Q,t)$ are called the intermediate scattering functions. For diffusive motion $S(Q,\omega)$ at a given Q is peaked at $\omega = 0$ and has to be observed as a broadening

Table I

polymer	solvent	concn × 10^2, g/mL	K^a per monomer unit in barns	$\bar{M}_w \times 10^{-3}$ [b]	R_g, Å	τ_1,[c] s
PS	C_6D_6	3.1	36	55	~70[d]	11.4×10^{-7}
PSD	CS_2	3.1	74	57	~70[e]	9×10^{-8}
PTHF	C_6D_6	3.0	30	~50	~148[d]	1.1×10^{-6}
PTDF	CS_2	3.1	50	~50	148[f]	7×10^{-7}
PDMS	C_6D_6	3.1	35	15	38[g]	2.2×10^{-8}

[a] $K = [\Sigma_p b - (v_p/v_s)\Sigma_s b]^2$, where $\Sigma_p b$ and $\Sigma_s b$ are the sum of scattering lengths and v_p and v_s the specific volumes of a monomer unit and a solvent molecule, respectively. [b] $\bar{M}_w$ determined by GPC (polystyrene calibration used for PTHF and PTDF). [c] τ_1 calculated from eq 1 using measured values of $R_g = (\langle r^2 \rangle/6)^{1/2}$. At 30 °C viscosity for CS_2 = 0.35 cP and viscosity for C_6D_6 = 0.56 cP.[28] [d] Estimated assuming ca. same solvent power for benzene and CS_2. [e] Estimated from ref 26. [f] Measured by SANS. [g] Taken from ref 27.

of the incident energy or wavelength distribution $\Delta\lambda$. Models are investigated via the variation of this broadening $\Delta\omega$ (which has to be deconvoluted from $\Delta\lambda$) with Q. The corresponding intermediate scattering functions are decaying correlation functions from which characteristic decay time constants, Ω, may be extracted directly and their variation with Q again compared with theory. The NSE technique has the great advantage for observation of diffusive motion of providing the intermediate scattering law directly. This removes the problem of deconvolution and provides a function often more easily compared with calculation. Most models lead to differences between $S_{inc}(Q,\omega)$ and $S_{coh}(Q,\omega)$ but in conventional experiments it is only possible to make one or other dominant by a judicious choice of scattering cross sections. The NSE technique, however, allows separation of the coherent and incoherent terms at the experimental stage.

At small Q, where $Q \sim 1/R_g$, the coherent intensity scattered by a polymer molecule is a function rising steeply as Q decreases, whereas the incoherent scattering is isotropic. The coherent cross section is governed by a contrast factor K[21]

$$K = [\sum_p b - (v_p/v_s)\sum_s b]^2 \text{ per polymer segment} \quad (6)$$

The subscripts p and s refer to a polymer segment and a solvent molecule, respectively. b is the neutron scattering length. The total intensity is then proportional to N_pK, where N_p is the number of segments per unit volume. The corresponding incoherent cross section would be just $N_p\sum_p(\langle b^2 \rangle - \langle b \rangle^2)$. The amplitude factor, b, in the nuclear scattering of neutrons varies from nucleus to nucleus and from isotope to isotope. In particular, $b = 0.667 \times 10^{-12}$ cm for deuterium and -0.35×10^{-12} cm for hydrogen. Thus suitable choice of solvent and, possibly, deuteration can give a very large value for K and hence for the coherent scattering intensity. The values of K for the polymer–solvent pairs investigated in these experiments are listed in Table I.

The intermediate scattering law $S_{coh}(Q,t)$, has been calculated by Dubois-Violette and de Gennes[5] for Zimm chains at intermediate Q ($QR_g > 1 > Qa$), where neither overall molecular size nor local structure is important.

The calculated $S_{coh}(Q,t)$ is a universal function of the normalized time coordinate $\mathcal{H}$ and has the form

$$S_{coh}(Q,t) = \mathcal{H}^{2/3}\int_0^\infty \exp\{-(\mathcal{H}^{2/3}u[1 + h(u)])\}\,du \quad (7)$$

where

$$h(u) = (4/\pi)\int_0^\infty ((\cos y^2)/y^3)[1 - \exp(-u^{-3/2}y^3)]\,dy$$

Akcasu et al.[19] have further developed the theory of scattering from a bead-and-spring model of a polymer in solution to cover continuously the whole range from molecular diffusion, through segmental motion (Q^3 region), to local bond rotation (which is represented by the diffusive motion of a single bead). The intermediate scattering law is expressed in terms of an inverse correlation time Ω defined as the first cumulant of the scattering law

$$\Omega = -\lim_{t\to 0} \frac{d \ln [S(Q,t)]}{dt} \quad (8)$$

The theory makes the same predictions as Dubois-Violette and de Gennes[5] for the region $1/R_g \ll Q \ll 1/a$, where

$$\Omega = 2^{1/2}(\mathcal{H}/t) = (1/6\pi)(k_BT/\eta_s)Q^3\ s^{-1} \quad (9)$$

This expression applies to Θ conditions. In a good solvent $S_{coh}(Q,t)$ has not been calculated but Ω shows the same Q^3 behavior with the numerical coefficient increasing[19] to 0.072. These calculations of Ω have been made by using a preaveraged Oseen tensor. It has been found[22] that preaveraging does not affect the overall behavior of Ω as a function of Q but that the numerical coefficient in eq 9 may vary by up to 10%.

At low Q ($QR_g \leq 1$) and frequencies ($\omega \leq 1/\tau_1$), Brownian diffusion (see for example Chapter 6 in ref 20) of the whole molecule dominates, and $S(Q,t)$ is a simple exponential of the form $e^{-\Omega t}$. Ω, which is proportional to Q^2, yields the temperature-dependent diffusion coefficient, $D(T) = \lim_{Q\to 0}(\Omega/Q^2)$, which is dependent on the molecular size. This behavior gradually gives way to Zimm-type internal motion as Q increases with a characteristic Q^3 dependence. At higher Q values ($Qa > 1$) and frequencies ($\omega \geq 10/\tau_1$), Ω deviates from Q^3 dependence, back to a Q^2 dependence as the local structure of the molecule becomes important. This region corresponds to the high-frequency results in viscoelastic measurements, where deviations from Zimm behavior are observed. As a simple first approximation the motion may be thought of as local Brownian motion of a single bead. As with increasing Qa the motion deviates from Q^3 behavior toward "local diffusion", so the shape of the intermediate scattering law, $S_{coh}(Q,t)$, is predicted to deviate from that given by Dubois-Violette and de Gennes (eq 7) for internal motion of Zimm chains toward the simple exponential form typical of diffusive motion of a single bead. Figure 2 shows the theoretical curve ln $[S_{coh}(Q,t)]$ vs. Ωt for Zimm chains (evaluated from eq 7 and 10) which is predicted to hold for values $Qa \leq 1$, together with ln $[S_{coh}(Q,t)]$ for Qa = 2, 4, and 6 (after ref 19). Also shown is the limiting straight line representing diffusive motion. The curves in Figure 3 have been taken from ref 19 and show the normalized inverse correlation time, $(\Omega/Q^2)(\eta_s a/k_BT)^{-1}$, against Qa calculated by using the Zimm model for polymers of different sizes and for different values of the draining parameter B, where

$$B = [1/(6\pi^2)^{1/2}](\xi_0/\eta_s a)$$

ξ_0 is the friction coefficient of a Gaussian bead spring of length a. B is in fact identical except for a factor $2^{1/2}$ to the reduced draining parameter $h^* = h/N^{1/2}$, where N is the number of beads and h is the parameter introduced by Zimm[3] to represent the degree of drainage of the solvent

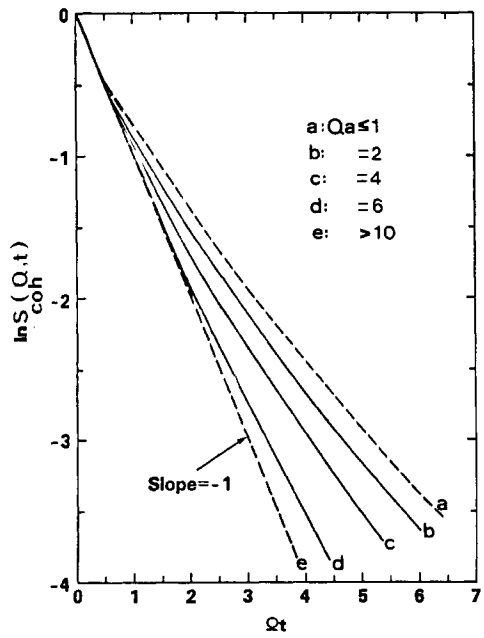

Figure 2. Theoretical correlation functions calculated for different values of Qa. $Qa < 1$ corresponds to eq 7 for Zimm motion; $Qa > 10$ corresponds to a simple exponential representing diffusion. The intermediate values are taken from ref 19.

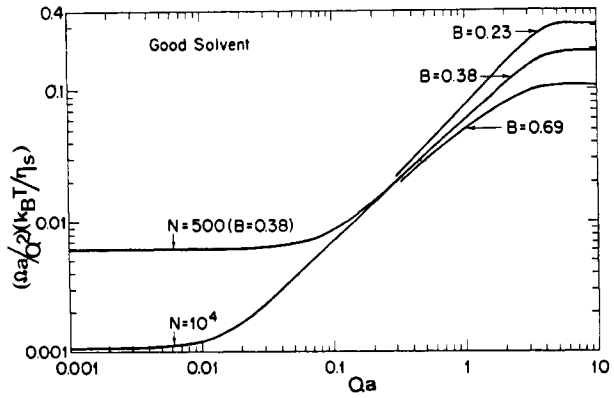

Figure 3. Variation of the normalized Ω values with normalized Q for different values of the draining parameter B and for two chain lengths in a good solvent (ref 19).

molecules through the polymer.[1] For the limit of free draining, $B = 2^{1/2}h^* = 0$. By fitting the experimental Ω data to these calculated curves, one can obtain values of a and B. Note that for any B value the curves for different-sized molecules (defined by the number of beads, N) coincide at high Qa, where overall molecular size is important. At low Qa, where molecular dimensions determine the rate of motion, the curves for different values of B coincide for given values of N.

The range of interest in these experiments covers the Q^3 region and the crossover to local motion, where the draining parameter has the most effect. The quality of the experimental data, however, precluded a two-parameter fit and led us to fix B and extract only one variable, a, the length per bead. The literature gives a number of estimates of h^*, most of which fall in the range 0.1–0.4 for typical polymers in solution.[6] Kirkwood and Riseman[23] calculated the ratio

$$f_0/(\eta_s\langle r^2\rangle^{1/2})$$

for a nondraining molecule, where f_0 is the molecular friction coefficient. For polymers of reasonable molecular weight, the ratio is $(3\pi)^{3/2}2^{-5/2}$ (see, for example, Yamakawa,[1] p 272). Equating the friction factor ξ_0 of a Gaussian subchain forming a bead–spring unit to that of a Gaussian molecule and using the Kirkwood–Riseman value of the friction ratio give $B = 0.38$ and correspondingly $h^* = 0.265$, well within the range of h^* values found suitable for polymers in solution. The Kirkwood–Riseman value of B was therefore used for all the calculations presented here.

3. Experimental Section

3.1. Samples. Table I lists the polymers and solvents used, together with the important physical parameters. Poly(tetrahydrofuran) (PTHF) and poly(tetrahydrofuran-d_8) (PTDF) were prepared from carefully purified monomers (AnalaR from BDH Ltd. and deuterated monomer from Merck Sharp and Dohme (99 atom % D)) and polymerized by using antimony pentachloride as the initiator, following the procedure described in ref 24.

The molecular weights were shown, by GPC analysis, to be about 50 000 with broad distributions. NMR examinations indicated that the deuterated polymer contained less than 1% PTHF and its radius of gyration, R_g, was measured in CS_2 by small-angle neutron scattering and shown to be 140 Å. As benzene is also a good solvent for this polymer, the same value is assumed for the PTHF dimensions in C_6D_6.

The samples of polystyrene (PS) and polystyrene-d_8 (PSD) were prepared anionically from styrene monomer and styrene-d_8 (from Aldrich Chemical Co.) in benzene at 25 °C, using n-butyllithium as initiator.[25] The molecular weights determined by GPC were 55 000 and 56 000 for PS and PSD, respectively, with $\bar{M}_w/\bar{M}_n$ = 1.24 and 1.25. The sample of poly(dimethylsiloxane) was kindly provided by Dr. J. A. Semlyen of York University. It was obtained by preparative GPC fractionation of Dow Corning DC 200 series Dimethicones and has molecular weight distribution parameter $\bar{M}_w/\bar{M}_n$ = 1.075.

All solutions were held in sealed quartz cans of optical path 8 mm. Unless otherwise stated, they were thermostatically controlled at 30 °C.

3.2. Apparatus. Experiments were carried out at the high-flux reactor at the Institut Laue-Langevin, Grenoble, France, using the IN11 spin-echo[13-16] spectrometer.[29a] This apparatus allows measurement of changes in the energy of neutrons scattered by a sample by changing and keeping track of the neutron beam polarization nonparallel to the magnetic guide field. The resultant neutron beam polarization, when normalized against a purely elastic scatterer (e.g., glassy polystyrene) is directly proportional to the cosine Fourier transform of the coherent scattering law, $S_{coh}(Q,\omega)$; i.e., the intermediate scattering law, or time correlation function, $S_{coh}(Q,t)$ is measured directly. Energy changes down to 0.01 μeV may be measured by this technique. The incident wavelength in these experiments was 8.3 Å with a spread $\Delta\lambda/\lambda$ of 10%. The Q values ranged from 0.026 to 0.16 Å^{-1}.

3.3. Data Analysis. Figure 2 shows that to obtain Ω from the measured correlation functions, $S_{coh}(Q,t)$ should be analyzed by using different theoretical functions for different ranges of Qa. Although use of the "initial slope" $\lim_{t\to 0}\{d \ln [S_{coh}(Q,t)]/dt\}$ to extract Ω removes the necessity of assuming a model for the correlation functions, the quality of the data (see, for example, correlation functions displayed in Figure 4) gives rise to unacceptable uncertainty in Ω values obtained in this way. The Akcasu correlation functions (Figure 2), however, cannot be fitted until a has been determined. Therefore as an initial approach the de Gennes correlation function (eq 7) was fitted to the data. The inverse correlation time $(\mathcal{H}/t)$ is the only variable to be fitted and the initial slope is then given by $\Omega = 2^{1/2}(\mathcal{H}/t)$ (see eq 9). The Ω values thus obtained were checked to see that they produced an acceptable initial slope to the data. The data (plotted as Ω/Q^2 vs. Q) were then fitted to the theoretical curve of Akcasu (see Figure 3) for the appropriate solvent conditions and solvent viscosity, with B fixed at 0.38. Both axes in Figure 3 are normalized by a so that the fit is made by sliding the data diagonally over the master curve, which is plotted for an arbitrary value of a.

In principle, an iterative process should then be used to "home in" on the final value of a and Ω. That is to say, knowing Qa, one can fit the appropriate Akcasu function (see Figure 2) to the data to obtain a new set of Ω values and hence a new value of a

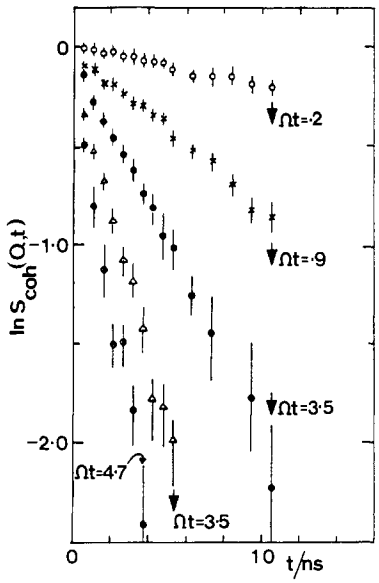

Figure 4. Normalized correlation functions plotted logarithmically against time for PS in CS_2. Q values are as follows: (ó) 0.026; (×) 0.05; (●) 0.08; (△) 0.11; (⊙) 0.13 Å^{-1}. The highest value reached for Ωt is marked on each curve.

by refitting to the master curve. However, the quality of the data already produces very large uncertainties in the initial Ω values and, hence, in the values of a obtained. The error bars at the second iteration cover much the same range as at the first stage and thus no real convergence is possible. A fit of a linear time dependence for ln $[S_{coh}(Q,t)]$ (characteristic of Brownian motion at very high Qa) must give the lower limiting value of Ω whereas de Gennes' correlation function gives the upper limit. At the highest experimental values of Qa the results of such a straight-line fit to ln $[S_{coh}(Q,t)]$ are shown in Figures 9 and 10 as an extension to the error bars.

3.4. Resolution in Time and in Q. A. Errors in Ω. Errors in the correlation functions $S_{coh}(Q,t)$ arise directly from the counting statistics in the sample, background, and normalization runs. Even with very long counting times statistical errors become prohibitive when $S_{coh}(Q,t)/S_{coh}(Q,0) \leq 0.1$ so data do not extend beyond this point.

Error bars are displayed with each correlation function. These error bars give rise to a range of possible values for Ω when fitting the theoretical de Gennes curve to $S_{coh}(Q,t)$. The maximum and minimum Ω values producing reasonable fits are used as the limits of the Ω error bars.

B. Errors in Q. The spin-echo technique achieves high-energy resolution without many of the usual flux penalties associated with special focusing techniques and allows the use of a broad incident wavelength spread ($\Delta\lambda/\lambda$ = 10%). This gives rather poor Q resolution. However, it has been shown[29b] that for systems where the correlation times vary with Q^3 (i.e., with $1/\lambda^3$) the effect of this on the values of Ω is very small due to a λ^3 variation of the Fourier time variable which appears in the detailed analysis of the spin-echo technique itself. Thus for most of the data presented here the wavelength resolution is not an important effect. There is another, more important, uncertainty in Q introduced via the angular collimation of the neutrons (this affects the definition of θ in eq 3). The experimental collimation was ±0.25° and, together with the wavelength spread, this leads to an uncertainty in the lowest values of Q of 14%, dropping to ±10% at the higher Q values.

4. Results

Figure 4 shows a set of normalized correlation functions obtained at 30 °C for PSD in CS_2 at five values of Q between 0.026 and 0.13 Å^{-1}, plotted logarithmically against time. None of the functions displayed show much curvature (as compared with Figure 2). At low Q, where the most curvature is expected (since Qa will be small), the Ωt range covered in the experiment only reaches 0.2 and

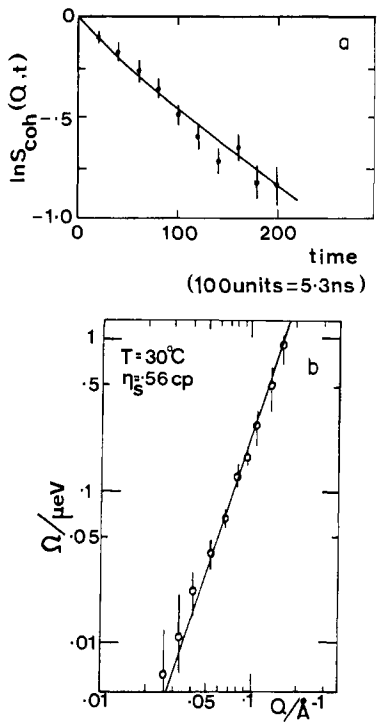

Figure 5. (a) ln $[S_{coh}(Q,t)]$ vs. t for PDMS in C_6D_6. The solid line is the fitted theoretical curve from eq 7 for $\mathcal{H}/t = \Omega/2^{1/2} = 7 \times 10^7$ Hz. (b) ln–ln plot of the inverse correlation time Ω against Q for PDMS in C_6D_6. The solid line is calculated from eq 9.

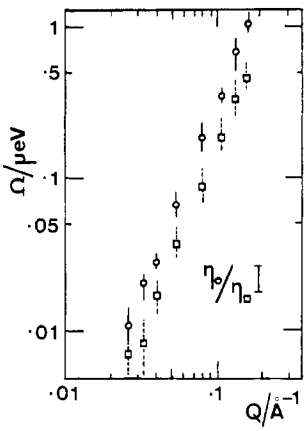

Figure 6. ln–ln plot of Ω against Q for (□) PS in C_6D_6 and (○) PSD in CS_2. The solid bar represents the ratio of the solvent viscosities on the same scale.

in this range all the functions in Figure 2 are approximately linear. At high Q the normalized time scale is longer and Ωt reaches 5 at Q = 0.13 Å^{-1}, but as Qa increases, the expected correlation function tends toward a simple exponential function. (The value of the step length a obtained by fitting the Ω values from these data to the master curve in Figure 3 is 38 Å. At Q = 0.13 Å^{-1}, $Qa \sim 5$ and ln $[S(Q,t)]$ is nearly linear in time as shown in Figure 2.)

Figure 5a shows data for PDMS in C_6D_6 at Q = 0.066 Å^{-1} fitted to the de Gennes curve and showing rather more curvature (for PDMS the value of a is 15 Å; Qa is of order unity and approximately Q^3 behavior is seen over most of th experimental range). In Figure 5b the values of Ω obtained from such fits to all the data for PDMS are displayed logarithmically against Q. The solid line is calculated from eq 9 with η_s = 0.56 cP and T = 30 °C. This equation applies for Θ conditions. Although these experiments are carried out approximately 40 °C above T_Θ for PDMS in C_6H_6, there is other experimental evidence

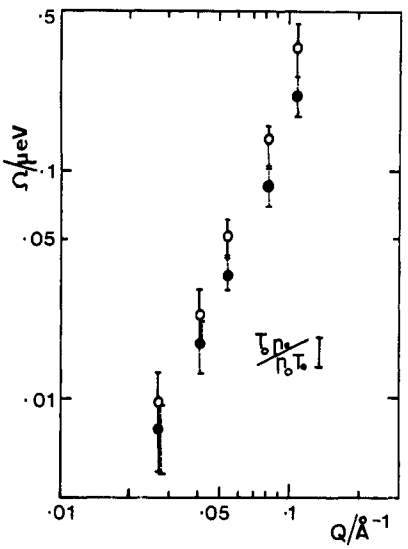

Figure 7. ln–ln plot of Ω against Q for PS in C_6D_6 at two temperatures: (○) 50 °C; (●) 30 °C. The solid bar represents the change in T/η_s.

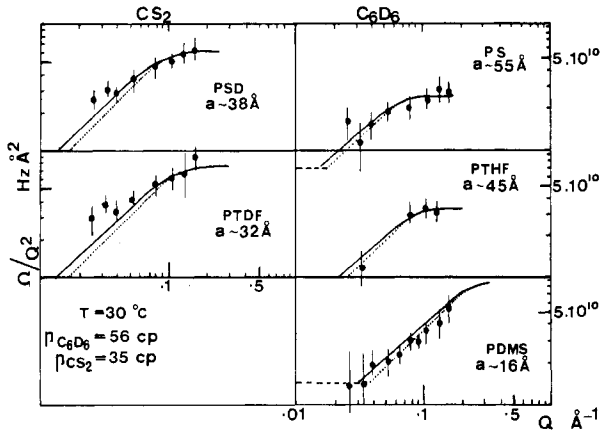

Figure 8. ln–ln plots of Ω/Q^2 against Q. The solid lines are fitted theoretical curves of Akcasu et al.[19] for a good solvent with B = 0.38. The dotted lines are the corresponding Θ curves. Solvent viscosities and the values of a extracted from the fits are shown in the figure.

that this temperature is not high enough for good-solvent conditions to apply in dynamic experiments.[17,35] Data for PS and PSD in Figures 6 and 7 do not show this simple Q^3 behavior. (This is more clearly seen in Figure 8.) The effect of changing solvent viscosity is shown in Figure 6, where results for PSD in CS_2 are compared to those for PS in C_6D_6. In the region of Q^3 behavior, eq 9 predicts a vertical shift proportional to η_s, the solvent viscosity. The extent of this shift for the solvents in question is shown as a vertical bar on the data and is seen to be somewhat smaller than the observed shift. Outside the Q^3 range, however, three possible variables, a, B, and η_s, may cause a more complex behavior. Simpler behavior may be anticipated if the solvent itself is not changed but the viscosity varied via the temperature (eq 9 predicts a shift proportional to T/η_s for the Q^3 range). Figure 7 shows data for PS in C_6D_6 at 30 and 50 °C and a vertical bar showing the change in T/η_s which agrees fairly well with the observed shift in the rate of motion. As explained in section 3.3, the Ω values displayed in Figures 5–7 were obtained by fitting the de Gennes curve to the data. Unlike the PDMS data, the polystyrene data in Figure 6 and 7 do not have a slope of 3 but exhibit a lower Q dependence of Ω. Deviations from the Q^3 dependence predicted by eq 9 are

Table II

solvent	polymer	a,[a] Å	Ω',[b] s^{-1}	D_{eff},[b] $cm^2\ s^{-1}$
C_6D_6	PS	55	0.8×10^8	2.3×10^{-6}
	PTHF	45	1.8×10^8	3.3×10^{-6}
	PDMS	15	4×10^9	9×10^{-6}
CS_2	PSD	38	4×10^8	6×10^{-6}
	PTDF	32	7×10^8	7×10^{-6}

[a] Errors in absolute values of a are of the order ±10 Å but the relative values for the different polymers are probably more reliable. [b] Errors in Ω' and D_{eff} are directly governed by those in a.

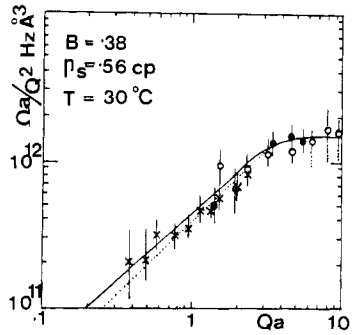

Figure 9. ln–ln plots of $\Omega a/Q^2$ against Qa for three polymers in C_6D_6: (○) PS; (●) PTHF; (×) PDMS. The solid curve is the theoretical curve for a good solvent of viscosity 0.56 cP at 30 °C and with B = 0.38.[19] The dotted curve is the corresponding Θ solvent curve.

more clearly seen when the variation of Ω/Q^2 is examined, as shown in Figure 8.

Only the PDMS data show Q^3 behavior; other samples show a slower Q dependence. Comparison of the data with the theoretical curves (discussed in section 3.4) allows values of a to be estimated. In Figure 8 the solid lines represent the curves for good-solvent conditions and the dotted lines those for Θ solvents. Examination of Figure 8 shows that while the PDMS data fall in the Q^3 region and show a better fit to the curve appropriate to Θ conditions, the data for PS and PTHF fall in a range where Θ- and good-solvent curves are indistinguishable. Table II lists the values of a extracted from these fits. It should be noted that since N is not fixed for a given polymer molecule until a is known ($N = 6R_g^2/a^2$), all the fits to the Akcasu theory for Ω/Q^2 have been made assuming $N = 10^4$. In the extreme low Q limit, however, N always appears in expressions for Ω so that only overall molecular dimensions are significant and Ω/Q^2 tend to D, the molecular diffusion coefficient. For polystyrene in C_6H_6, light scattering measurements have given the variation of D with molecular weight and concentration.[30] The value of D for a polystyrene solution of the appropriate molecular weight and concentration is shown as a dashed line on the PS/C_6D_6 data in Figure 8. Diffusion data have also been published for PDMS in toluene,[31] which is a very similar solvent to benzene. In this case the concentration dependence of D was not given but was said to be "small". With suitable corrections of solvent viscosity and temperature we have therefore used the value of D from ref 31 for a 1.5% solution (somewhat smaller than our concentration) to show the level for diffusive motion in Figure 8. This dashed line on the PDMS/C_6D_6 data in Figure 8 shows that the lowest Q data are already impinging on the region of overall molecular diffusion for this rather small molecule.

Normalization of the Ω/Q^2 and the Q axes by the appropriate value allows all the data for a particular solvent (and temperature) to be displayed on one master curve. Figures 9 and 10 show the master curves for C_6D_6 and for

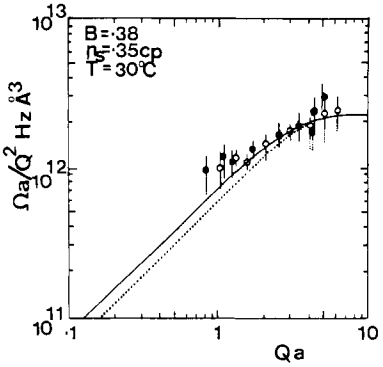

Figure 10. ln–ln plots of $\Omega a/Q^2$ against Qa for two polymers in CS_2: (○) PSD; (●) PTDF. The solid curve is the theoretical curve for a good solvent of viscosity 0.35 cP at 30 °C and with $B = 0.38$.[19] The dotted line corresponds to θ conditions.

CS_2 solutions, respectively (always fitting B at 0.38). These curves show clearly the systematic deviations from Q^3 behavior at higher values of Qa for the PS and PTHF data. As described in section 3.3, it is necessary to reexamine the analysis of this high-Q data in terms of the curves in Figure 2. Figure 2 shows that significant deviations from the de Gennes curve used in the initial data analysis are to be expected when $Qa > 3$. As explained in section 3.3, the uncertainties in a and Ω are too large for significant improvement to be made by using the Akcasu curves of Figure 2. To show the limiting case, the error bars for data above $Qa = 3$ have been extended by dotted lines to include the values of Ω which would be obtained from a straight-line fit (limit as $Qa \to \infty$) to ln $[S_{coh}(Q,t)]$. The sliding fits to the master curve are not significantly changed by these extensions so that the a values remain within the limits of the first iteration.

Once a has been fixed for a given polymer, another parameter available from the master curve is the value of Ω/Q^2 at the high-Q limit. Ω/Q^2 has the dimensions of a diffusion coefficient and values of $\lim_{Q\to\infty}(\Omega/Q^2)$ have been listed in Table II as D_{eff}. We also calculate a frequency Ω′ associated with the onset of the high-frequency Brownian behavior. Ω′ is calculated as Q'^2D_{eff}, where Q' is defined as the point where an extrapolation from the Q^3 region in Figure 3 crosses the horizontal line of high-Q behavior (approximately $Q' = 3.3/a$).

5. Discussion

The master curves displayed in Figures 9 and 10 demonstrate the ability of the simple bead–spring model when extended into the range $Qa > 1$ to explain the behavior of the inverse correlation time, Ω, over a wide frequency range. The fitting parameter, a, is the length of chain per bead in the model. Its variation for the different polymers studied in some sense reflects the differences in their local flexibility. Within the experimental error we place no significance on the differences in a values observed for the same polymer in different solvents. The related parameters Ω′ and D_{eff} reflect the same properties as a and we note that the ratio of D_{eff}/D_s (where D_s, the diffusion coefficient of the solvent, is 2.2×10^5 cm^2 s^{-1} for C_6H_6[32] at 30 °C) ranges from 0.1 for PS to 0.4 for PDMS, both in C_6D_6.

Comparison of Figures 8–10 shows that data for any one sample cover only a rather limited section of the overall behavior—PDMS data lie largely in the Q^3 range with the highest value of $Qa < 2$ while for PS the lowest Qa is >1 and no Q^3 region is observed. Observation at lower Q values is restricted by the resolution of the apparatus. (It is clearly not feasible to analyze a correlation function much flatter than the one for $Q = 0.026$ Å^{-1} shown in Figure 4 without markedly extending the time scale. Here, purely physical limitations on the functioning of the apparatus eventually come into play.) At high Q values the experiments are limited by counting statistics in two ways. First, the coherent structure factor $S_{coh}(Q)$ drops off sharply as Q increases and becomes comparable to the isotropic incoherent scattering so that the signal-to-noise ratio becomes very unfavorable. This limitation varies slightly, depending on the conformation of the particular polymer chain. Second, at high Q the correlation functions show fast time dependences so that $S_{coh}(Q,t)/S_{coh}(Q,0) < 0.1$ after only a few data points and again the signal is lost in the noise.

While the experimental Q range is essentially limited, the section of the Qa scale observed can be varied by choosing polymers with different values of a and/or R_g, thus bringing the different types of polymeric motion into range. (For somewhat smaller PDMS molecules than those used here even the overall diffusive motion may be observed.[33]) It is interesting to note that for small molecules, or very stiff polymers, the limits $Qa = 1$ and $QR_g = 1$ will approach each other and the true region of Q^3 behavior may effectively disappear. For the polymers discussed here, N $(=6R_g^2/a^2)$ is about 20 for PS, 200 for PHTF, and 400 for PDMS. Thus for the polystyrene no Q^3 region could be observed if data were extended to lower Q, as is confirmed by the proximity of the overall diffusion line to the data for PS in C_6D_6 shown in Figure 8. On the other hand, the smaller a value for PDMS gives rise to an extensive region of Q^3 behavior even for relatively small molecules. To explore the limiting high-frequency behavior in the region around $Qa = 1$ for this polymer requires measurement which falls outside the range of the spin-echo technique for the reasons described above.

Assuming that change of solvent affects only the viscosity in eq 9 and the ordinate of Figure 3, it is possible to compare these neutron data with the results of high-frequency viscoelastic data (see, for example, the work of Schrag et al.[6,34]). These visoelastic measurements are made in the kilohertz range by using highly viscous solvents having typical viscosities of 70 P at 25 °C. High-frequency limiting behavior sets in for polystyrene in such a solvent at 10^4 Hz. A direct conversion to benzene, using the ratio of solvent viscosities, gives a frequency of the order 10^8 Hz, exactly in the region of the Ω′ values listed in Table II.

The onset of high-frequency viscoelastic limiting behavior apparently corresponds to the onset of the limiting Q^2 behavior in neutron scattering experiments. The neutron experiments demonstrate explicitly that this corresponds to exploration of a distance scale smaller than the length of one spring. A single spring length has been estimated from viscoelastic measurement to contain 11 polystyrene monomers.[6] If we use the relationship $aN^{1/2} = 6^{1/2}R_g$ (which does not strictly apply here since we have good-solvent conditions) to obtain the number N of beads per chain, then from Tables I and II the length a contains 55, 11, and 5 monomers of PS, PTHF, and PDMS, respectively, in C_6D_6. Our estimate of the bead size a is thus rather larger than that obtained from viscoelastic measurements, for polystyrene at least.

Although resolution considerations at present preclude discussion of the high Q data in terms of detailed models based on local bond rotation, it is interesting to compare the neutron correlation times with those obtained by other methods which explicitly explore local rearrangement of the chain backbone. Matsuo et al.[36] compared the relaxation times obtained with data for polystyrene in solution from a number of techniques. Analysis of ^{19}F NMR and

^{13}C NMR T_1 relaxation data and nuclear Overhauser enhancement in terms of three-bond rearrangements as the dominant relaxation mode[36,37] gave correlation times of the order 0.27×10^{-9} s for PS in C_6D_6 at 30 °C. Comparison with the neutron results in Figure 8 shows this corresponds to data at Q values of the order 0.4 $Å^{-1}$—i.e., to exploration of distances of the order 2–3 Å. Such distances are certainly compatible with a three-bond relaxation mode. On the other hand, dielectric relaxation[38] and fluorescence depolarization experiments[39] produce correlation times an order of magnitude longer at about 4×10^{-9} s for PS in benzene. In the neutron experiments this corresponds to a distance scale of 10 Å ($Q \approx 0.1$ $Å^{-1}$). These techniques are apparently sensitive to backbone rearrangements of longer segments. The importance of the neutron data is that they provide explicit information about the distance scale corresponding to the observed frequencies. Improvement in the precision of the high Q neutron data will be best made by using more conventional neutron scattering techniques and these will be more easily analyzed now that there is a satisfactory picture of the whole frequency range of scattering from polymers in solution. Comparison of data from all the available techniques will then allow a better understanding of the nature of the local motion and of the parameter a.

Acknowledgment. We are indebted to Dr. R. H. Hall for preparation of the samples. Drs. D. Rimmer (ILL, Grenoble) and J. Perkins (Department of Chemical Engineering and Chemical Technology, Imperial College) provided essential help with calculations of the correlation functions. Discussions with Dr. C. Han (National Bureau of Standards) and Professor A. Z. Akcasu (University of Michigan, Ann Arbor) form the background to the interpretation of data presented here, and we are most grateful to them for their patience and hospitality. L.K.N. is indebted to the Science Research Council for the research grant supporting this work.

References and Notes

(1) Yamakawa, H. "Modern Theory of Polymer Solutions"; Harper and Row: New York, 1971.
(2) Rouse, P. E., Jr. *J. Chem. Phys.* **1953**, *21*, 1272.
(3) Zimm, B. H. *J. Chem. Phys.* **1956**, *24*, 269.
(4) Pecora, R. *J. Chem. Phys.* **1968**, *49*, 1032.
(5) (a) de Gennes, P. G. *Physics (Long Island City, N.Y.)* **1967**, *3*, 37. (b) Dubois-Violette, E.; de Gennes, P. G. *Physics (Long Island City, N.Y.)* **1967**, *3*, 181.
(6) Osaki, K.; Schrag, J. L. *Polym. J.* **1971**, *2*, 541.
(7) Berne, B. J.; Pecora, R. "Dynamic Light Scattering, with Applications to Chemistry, Biology and Physics"; Wiley: New York, 1976.
(8) Higgins, J. S. *Treatise Mater. Sci. Technol.* **1979**, *15*, 381.
(9) Adam, M.; Delsanti, M. *Macromolecules* **1977**, *10*, 1229.
(10) Allen, G.; Ghosh, R. E.; Higgins, J. S.; Cotton, J. P.; Jannink, G.; Weill, G. *Chem. Phys. Lett.* **1976**, *38*, 577.
(11) Higgins, J. S.; Ghosh, R. E.; Howells, W. S.; Farnoux, B.; Weill, G. *Chem. Phys. Lett.* **1977**, *49*, 197.
(12) Akcasu, A. Z.; Higgins, J. S. *J. Polym. Sci., Polym. Phys. Ed.* **1977**, *15*, 1745.
(13) Mezei, F. *Z. Phys.* **1972**, *255*, 146.
(14) Hayter, J. B. In "Neutron Diffraction"; Dachs, H., Ed.; Springer-Verlag: Berlin, 1978.
(15) Hayter, J. B. *Z. Phys.* **1978**, *B31*, 117. *Ibid.* **1979**, *B35*, 199.
(16) Nicholson, L. K., to appear in *Contemp. Phys.*
(17) Richter, D.; Hayter, J. B.; Mezei, F.; Ewen, B. *Phys. Rev. Lett.* **1978**, *41*, 1484.
(18) Higgins, J. S.; Nicholson, L. K.; Hayter, J. B. *Polymer* **1981**, *22*, 163.
(19) Akcasu, A. Z.; Benmouna, M.; Han, C. C. *Polymer* **1980**, *21*, 866.
(20) Willis, B. T. M. "Chemical Applications of Thermal Neutron Scattering"; Oxford University Press: London, 1973.
(21) Higgins, J. S.; Stein, R. S. *J. Appl. Crystallogr.* **1978**, *11*, 346.
(22) Benmouna, M.; Akcasu, A. Z. *Macromolecules* **1980**, *13*, 409.
(23) Kirkwood, J. G.; Riseman, J. *J. Chem. Phys.* **1948**, *16*, 565.
(24) Braun, D.; Cherdron, H.; Kern, W. "Techniques of Polymer Synthesis Characterization"; Wiley-Interscience: New York, 1972.
(25) Morton, M.; Rembaum, A. A.; Hall, J. L. *J. Polym. Sci., Part A* **1963**, *1*, 461.
(26) Cotton, J. P.; Decker, D.; Farnoux, B.; Higgins, J. S.; Jannink, G.; Ober, R.; Picot, C.; des Cloizeaux, J. *Macromolecules* **1974**, *7*, 863.
(27) Higgins, J. S.; Dodgson, K.; Semlyen, J. A. *Polymer* **1979**, *20*, 553.
(28) "Handbook of Chemistry and Physics"; 59th ed.; Chemical Rubber Co.: Cleveland, Ohio, 1979.
(29) (a) Dagleish, P.; Hayter, J. B.; Mezei, F. "Neutron Spin-Echo"; Mezei, F., Ed.; Springer-Verlag: Berlin, 1980. (b) Hayter, J. B. *Physica* **1980**, *128*.
(30) Adams, M.; Delsanti, M. *J. Phys.* **1976**, *37*, 1045.
(31) Edwards, C. J. C.; Stepto, R. F. T.; Semlyen, J. A. *Polymer* **1980**, *21*, 781.
(32) Rathbun, R.; Babb, A. *J. Phys. Chem.* **1961**, *65*, 1072.
(33) Higgins, J. S.; Nicholson, L. K.; Hayter, J. B. *Polym. Prepr., Am. Chem. Soc., Div. Polym. Chem.* **1981**, *22*, 86.
(34) Brueggman, B. G.; Minnick, M. G.; Schrag, J. L. *Macromolecules* **1978**, *11*, 119.
(35) Richter, D.; Ewen, B.; Heidemann, A. *Macromolecules* **1980**, *13*, 876.
(36) Matsuo, K.; Kuhlman, K. F.; Yang, W.-H.; Geny, F.; Stockmayer, W. H.; Jones, A. A. *J. Polym. Sci., Polym. Phys. Ed.* **1977**, *15*, 1347.
(37) Schaefer, J.; Natusch, D. F. S. *Macromolecules* **1972**, *5*, 416.
(38) Mashimo, S.; Chiba, A. *Polym. J.* **1973**, *5*, 41.
(39) Biddle, D.; Nordström, T. *Ark. Kemi* **1970**, *32*, 359.